THE JOURNAL OF PHYSICAL CHEMISTRY C

Article

pubs.acs.org/JPCC

Plasmonic-Heating-Induced Nanoscale Phase Separation of Free Poly(*N*-isopropylacrylamide) Molecules

Issei Aibara, Shinya Mukai, and Shuichi Hashimoto*

Department of Optical Science and Technology, University of Tokushima, 2-1 Minami-Josanjima, Tokushima 770-8506, Japan

Supporting Information

ABSTRACT: The localized-surface-plasmon resonance (LSPR) of gold nanoparticles (Au NPs) depends sensitively on the environmental refractive index. We found that LSPRs of single Au NPs supported on a transparent substrate can monitor the phase transition/separation of thermoresponsive poly(*N*-isopropylacrylamide) (PNIPAM) in aqueous solution. Both reversible and irreversible phase separations were observed. Plasmonic-heating-induced redshifts and subsequent cooling-induced recovery were observed on a glass substrate. Besides reversible redshifts at lower laser intensities, permanent redshifts were evident at higher intensities after illumination on a sapphire substrate, which has a much higher thermal conductivity than glass. The permanent redshifts were caused by the formation of a PNIPAM shell around the NP. For this permanent aggregation, temperature shaping around the Au NP by the substrate was found decisively and may find new chemistry applications based on local temperature landscapes. The observed nanofabrication of core−shell particles is one such example.

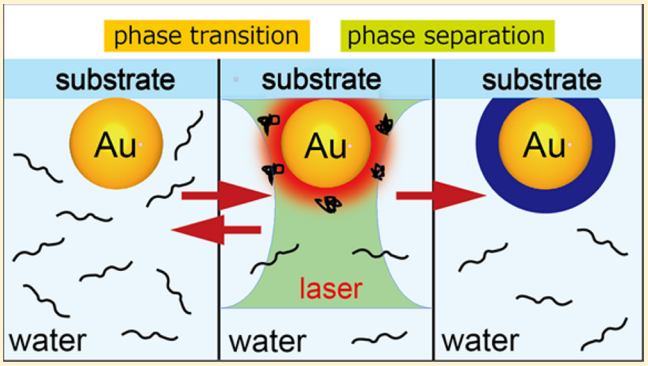

1. INTRODUCTION

Light interacts with the conduction electrons of plasmonic nanoparticles, resonantly exciting their coherent oscillations. The phenomenon is known as localized surface plasmon resonance (LSPR) and is the origin of the strong absorption/scattering of incident light by nanoparticles such as those composed of gold (Au NPs).[1] LSPRs decay both radiatively and nonradiatively. The former is responsible for the plasmonic enhancement of the electric field in the near-field regime, whereas the latter decay contributes to particle heating and subsequent heat transfer from the particle to the surrounding medium.[2−4] Because NP volumes are tiny compared with the bulk, heating of the medium is extremely localized; this is the most remarkable feature of plasmonic heating.[5,6] This localized heating has made Au NPs an ideal candidate for photothermal cancer therapy.[7,8] Recently, plasmonic heating by Au NPs and nanostructures (NSs) has emerged as an innovative method for manipulation and fabrication at the micro- to nanoscale. For instance, particle elongation occurs when a Au NP is exposed to a focused Gaussian laser beam because of melting and radiation pressure.[9] A gradient force squeezes the particle perpendicular to the laser beam, and a scattering force pulls the particle in the direction of beam propagation. Photothermally triggered one-dimensional self-assembly was also observed to occur for poly(*N*-isopropylacrylamide) (PNIPAM)-functionalized gold nanorods through an increase in temperature of the system.[10] Various methods of plasmonic heating-based control and chemistry have been developed.[11,12]

Plasmonic heating has been shown to cause phase transitions in surrounding media such as vapor bubble formation at ambient pressure and supercritical transition under high pressure, which was monitored by LSPR extinction spectra.[13−15] Subsequently, we developed a keen interest in phase transitions of solute molecules dissolved in solutions; phase transitions can be driven through plasmonic heating of NPs, a mechanism that had not been explored previously. Such plasmonic heating-induced phase transitions of solutes can be tested by PNIPAM which is a well-investigated water-soluble thermoresponsive polymer. At room temperature, PNIPAM dissolves in water in a random coil state forming a homogeneous phase; when heated to temperatures above 32 °C (305 K), the lower critical solution temperature (LCST), a phase transition occurs from coil to globule state.[16,17] The globular molecules aggregate because of hydrophobic interactions, resulting in a phase separation with the solution turning turbid.

Here we report reversible and irreversible plasmonic-heating-induced phase separation/aggregation of PNIPAM monitored using single-particle LSPR spectra. We used particles supported on a substrate and exposed to a PNIPAM solution. This substrate is pivotal in controlling the medium temperature field around a Au NP and thus dictates the phase separation of PNIPAM.

Received: April 27, 2016
Revised: July 6, 2016

DOI: 10.1021/acs.jpcc.6b04265
J. Phys. Chem. C XXXX, XXX, XXX−XXX

2. EXPERIMENTAL SECTION

The single-particle scattering spectra were measured by dark-field microscopy−spectroscopy (Scheme 1) at a wavelength

Scheme 1. Experimental Configuration

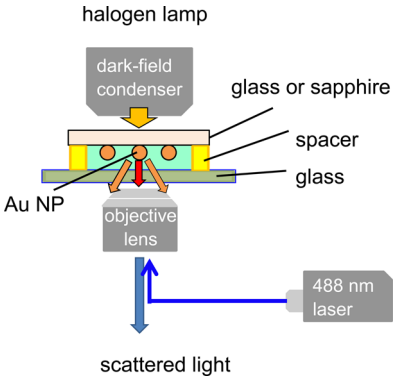

resolution of 0.5 nm. A halogen lamp with a broad (white) spectrum was used for illumination when recording the scattering spectra. The particles were heated by illuminating a focused 488 nm CW laser, OBIS-488-LX-150 (Coherent, Santa Clara, CA), beam through a microscope objective (60 ×, NA = 0.70) on an inverted microscope, IX-71 (Olympus, Tokyo, Japan). Poly(*N*-isopropylacrylamide) (PNIPAM) (MW: 20 000−40 000: Sigma-Aldrich Co., St. Louis, MO) and polyvinylpyrrolidone (PVP) (K-30, MW: 40 000; Tokyo Kasei Co., Tokyo, Japan) were used as received. Aqueous solutions of Au NPs with nominal diameters of 100 nm (EMGC100: BBI Solutions, Cardiff, UK) were transformed from faceted to spherical shape by irradiating with weak-intensity nanosecond laser pulses (≈11 mJ cm^{-2}) of 532 nm wavelength. The particle image acquired using a transmission electron microscope and the corresponding size distribution (104 ± 6 nm) are given in Supporting Information S1. Spherical Au NPs were spin-coated onto an optically polished 0.5 mm thick sapphire substrate (Shinkosha, Yokohama, Japan) or a 0.17 mm thick borosilicate cover glass (Matsunami, Osaka, Japan). Au NPs were immersed in solutions of PNIPAM and PVP in an 11 μL chamber consisting of a sapphire or glass substrate, a 0.2 mm thick silicone rubber spacer, and a microscope coverslip. Further details of the procedure can be found in Supporting Information S2.

3. RESULTS AND DISCUSSION

A. Observation of Reversible and Irreversible LSPR Shifts. First, under a dark-field microscope, we exposed a 100 nm diameter spherical Au NP on a glass substrate to focused laser illumination of 488 nm wavelength in 1.0% aqueous PNIPAM solution. We recorded single-particle Rayleigh scattering spectra[18] before, during, and after illumination. Figure 1a shows the spectral changes originating from the heating of a Au NP. Before irradiation, LSPR scattering occurred with a spectral peak at λ_{max} = 578 ± 4 nm. At a laser peak power density of 0.18 mW μm^{-2} (1.8 × 10^4 W cm^{-2}), the spectral shift was within experimental error, whereas appreciable redshifts at 0.35 mW μm^{-2} and at 0.53 mW μm^{-2} were recorded. Notably, the shifts occurred only during illumination, and when stopped, the original spectra returned. The shifts were accompanied by spectral intensification, suggesting that their origin is ascribed to the increased refractive index sensed by a Au NP.[19,20] Figure 1b shows the histograms of the scattering spectral peak positions for 10 particles to check particle-to-particle difference. The statistical errors for the peak positions for 10 particles were not very small for the experimental peak-wavelength reproducibility of within 1 nm. This may arise from the small variation in NP size (104 ± 6 nm), particle-to-particle differences in focusing the laser, and possibly the varying geometry of the particle−substrate surface contact because of the surface roughness. The surface roughness of a glass substrate was measured using atomic force microscopy (AFM), giving an average roughness of 0.19 nm and a peak-to-valley roughness of 1.1 nm. These factors may produce differing particle temperatures for irradiations with the same laser intensity. Nevertheless, the basic conclusion holds: spectral shifts are greater for higher laser intensities. Most importantly, peak shifts are reversible, and the same peak shifts were observed for particle heating−cooling cycles at the same laser intensity (Figure 1c). In contrast, the observation of reversible redshifts was absent for aqueous 4.0% PVP solution (Supporting Information S3) when Au NPs supported on a glass substrate were exposed to illuminations of up to 5.3 mW μm^{-2}, a 10-fold increase in laser power density compared to that used for 1.0% PNIPAM solution.

The phenomenon we observed is interpreted as a LCST-induced aggregation of PNIPAM around the NP caused by the heating of the surrounding medium through heat transfer from the optically heated NP. Previously, the microscopically observed phase transition resulted in microparticles forming when PNIPAM solutions were directly heated with a focused infrared laser.[21−23] The present LSPR-based spectroscopic sensing of the phase separation of free PNIPAM is unprecedented. PNIPAM molecules are hydrophilic at temperatures below the LCST (305 K) but hydrophobic above LCST.[16] The phase transition and aggregation of PNIPAM increase the refractive index of the medium sensed by a Au NP, resulting in LSPR redshifts. Remarkably, we did not use PNIPAM molecules that were chemically attached to the Au NP. Nonetheless, we observed appreciable LSPR redshifts greater than those observed for PNIPAM-coated Au NPs that were heated to temperatures above the LCST.[24,25] For instance, for a colloidal solution of 8 kDa PNIPAM-Au NPs (13 nm-diameter Au NP coated with PNIPAM), the extinction maximum of the plasmonic band of 530 nm at 25 °C (298 K) shifted to 541 nm after heating to 40 °C (313 K).[25]

As will be described in Section B, increasing the laser intensity may raise the temperature of a Au NP to a level that causes temperature-induced changes to PNIPAM. To avoid this problem, we used a sapphire substrate with a remarkable cooling effect on a Au NP.[26] We observed reversible redshifts for 0.5% PNIPAM solution at 0.53−2.6 mW μm^{-2} (Supporting Information S4). Besides this observation, we observed irreversible redshifts at higher laser intensities.

Figure 2a shows the scattering spectrum before irradiation in 4.0% PNIPAM solution; Figure 2b shows the spectral change originating from irradiation at 5.3 mW μm^{-2} for 8 s for the same PNIPAM concentration. The insets are particle images from the scanning electron microscopy (SEM). The laser irradiation permitted the observation of a permanent scattering spectral redshift, and this was ascribed to the increase in particle size resulting from the growth of a shell around the Au NP, as revealed by SEM images as well as AFM particle height profiles (Supporting Information S5). For a number of particles, we measured the spectral peak position as a function of particle

DOI: 10.1021/acs.jpcc.6b04265
J. Phys. Chem. C XXXX, XXX, XXX−XXX

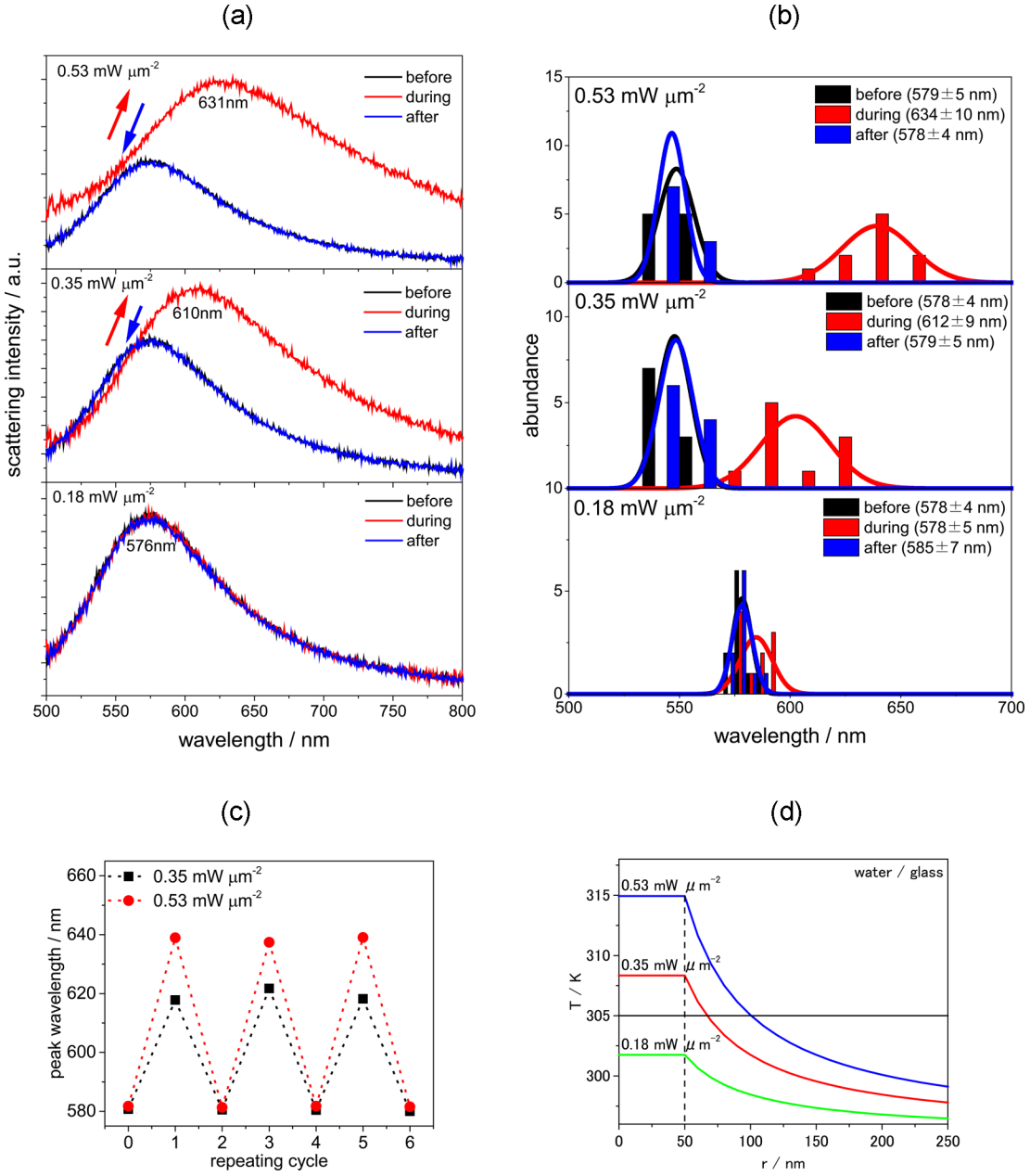

Figure 1. *In situ* scattering spectral changes: before, during, and after laser illumination of a 100 nm diameter Au NP supported on a glass substrate and submerged in aqueous solution of 1.0% PNIPAM: (a) scattering spectra during the illumination of 488 nm laser light at laser peak power densities, 0.18, 0.35, and 0.53 mW μm^{-2}, together with spectra before and after irradiation; (b) histograms of scattering spectral peak positions for 10 particles at the three laser peak power densities. During laser illumination, redshifts occurred for the two higher densities but shifted back after illumination. (c) Reversibility in the LSPR peak position over the duty cycle of illumination. (CCD sampling time) × (exposure) was 0.4 s × 10. The experimental temperature was 295 ± 1 K. (d) Calculated radial temperature distribution in water for irradiation of a 100 nm diameter Au sphere supported on a glass substrate at experimental laser peak power densities (see Section B for details).

diameter from the SEM micrographs (Figure 2c). This result supports the hypothesis of a core−shell formation because the numerical simulation of scattering cross-section spectra using COMSOL Multiphysics (Supporting Information S6) gave a shell-thickness dependence of peak position similar to the experiment. In the simulation, we used a model in which a Au core−PNIPAM shell concentric structure is supported on a substrate (see Supporting Information S6). Figure 2d shows the peak shift as a function of exposure time at various PNIPAM concentrations. The accumulation and aggregation of PNIPAM on Au NP depend on the PNIPAM concentration: shell formation can be faster at higher concentrations. Figure 2e shows the laser peak power-dependent shell thickness represented by a peak shift as a function of the exposure time. The threshold was found at 3 mW μm^{-2} for 4.0% PNIPAM, and the rate of shell growth was higher for higher laser peak power density. Finally, to estimate the difference in the rate of shell growth for PNIPAM from that for a nonthermosensitive polymer, we compared those rates for PNIPAM and polyvinylpyrrolidone (PVP). The PVP shell growth rate measured by LSPR scattering peak shift (Figure 2f) was much slower than that of PNIPAM. We actually observed shell formation for PVP (Supporting Information S7) from SEM micrographs. At the highest fluence of 5.3 mW μm^{-2},

DOI: 10.1021/acs.jpcc.6b04265
J. Phys. Chem. C XXXX, XXX, XXX−XXX

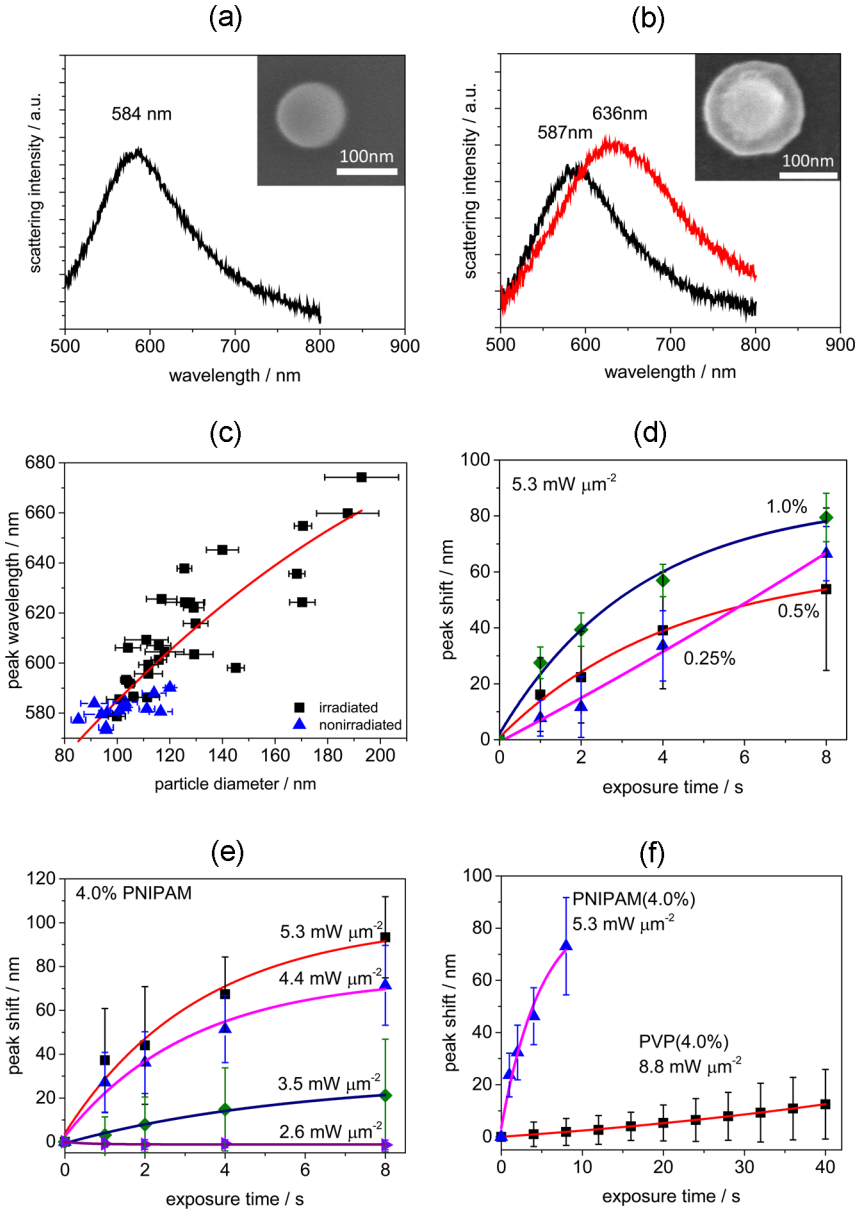

Figure 2. (a, b) Single-particle scattering spectrum with corresponding SEM image (inset) of (a) pristine Au NP and (b) subsequent changes arising from laser illumination after irradiation at 5.3 mW μm^{-2} for 8 s. (c) Correlation of scattering peak position with diameter for PNIPAM obtained from SEM images. (d–f) Scattering peak shifts (from averages of 15 particles) as a function of exposure time in various experimental conditions: (d) at various PNIPAM concentrations under the same illumination, (e) with the same PNIPAM concentration at various laser intensities, and (f) under different illuminations to compare shell growth rates of PNIPAM and PVP. The threshold laser peak power density for particle melting was 10.6 mW μm^{-2}. The solid curves in c–f are drawn as visual guides. Excitation wavelength: 488 nm.

particle melting or vapor bubble formation was absent during irradiation, suggesting that the observed spectral changes were brought about in liquid solely from the shell formation triggered by the laser-induced aggregation of PNIPAM. We failed to observe permanent encapsulation on a glass substrate below 3.5 mW μm^{-2} (Supporting Information S8).

B. Mechanistic Aspect from Temperature Estimation. Here we consider the origin of the spectral shifts observed on laser illumination, resulting in the particle heating and subsequent medium heating. The big difference between sapphire and glass is the heating efficiency of the Au NP arising from sapphire's much greater thermal conductivity, $k_{sapphire}$ = 42 W m^{-1} K^{-1}, than that of borosilicate glass, k_{glass} = 1.0 W m^{-1} K^{-1}. A numerical simulation was performed using COMSOL Multiphysics 5.1 given conditions of steady-state heating with simultaneous cooling by the medium and substrate.[26] Using the 2D temperature distribution (Figure 3a), the laser peak power density vs particle temperature obtained (Figure 3b) is linear with a slope three times greater for the glass substrate. From experiments with a glass substrate, the estimated particle temperature is 302 K for 0.18 mW μm^{-2}, 308 K for 0.35 mW μm^{-2}, and 315 K for 0.53 mW μm^{-2} obtained from Figure 3b. These estimated temperatures suggest that the phase separation of PNIPAM can occur for 0.35 and 0.53 mW μm^{-2} at which the particle and the medium immediately surrounding the NP are heated above the LCST of PNIPAM, i.e., 305 K. From the medium layer thickness where temperatures are above 305 K, we estimated the

DOI: 10.1021/acs.jpcc.6b04265
J. Phys. Chem. C XXXX, XXX, XXX−XXX

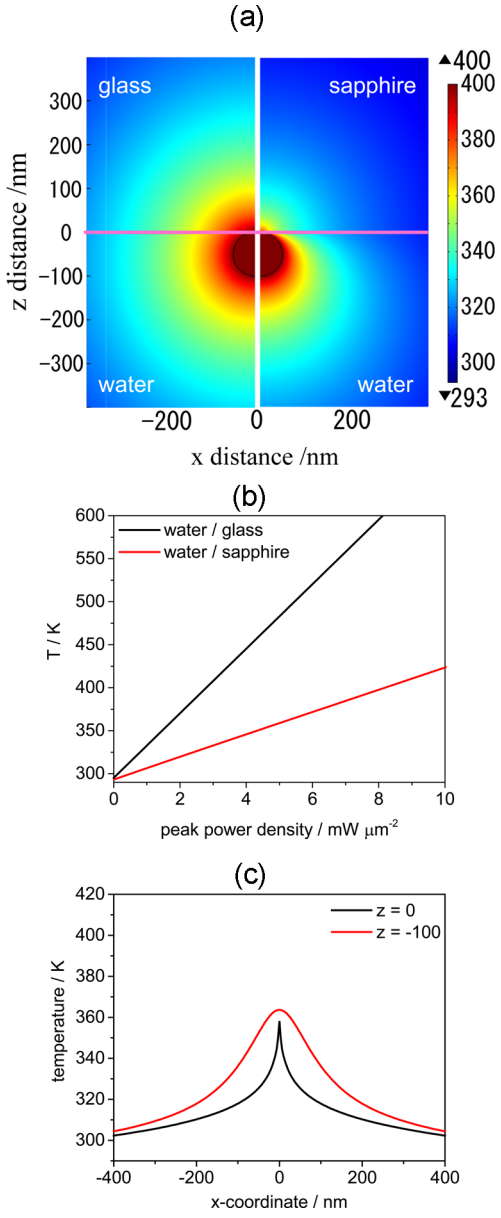

Figure 3. (a) 2D temperature distributions for water-immersed 100 nm Au NP on glass (left side) and on sapphire (right side), under optical illumination from a CW laser. Experimentally, we used up beam to illuminate a Au NP present on the top wall (ceiling) of the sample chamber. (b) Calculated particle temperature as a function of applied laser peak power density for a water-immersed 100 nm Au NP on sapphire (red line) and glass (black line) substrates. Note that the water temperature is the same as the particle temperature at the NP surface. To calculate temperature, we used the thermal conductivity of water because the PNIPAM contribution is minor. (c) Calculated 1D temperature profiles along upper (z = 0) and lower (z = −100 nm) sides of the particle (100 nm diameter), showing that a Au NP supported on sapphire substrate is cooler on the upper side (laser peak power density: 5.3 mW μm^{-2}).

thickness of the phase-separated PNIPAM aggregates (Table 1) assuming a core−shell supported on a substrate (Supporting Information S6). The steady-state medium temperature profiles (Figure 1d) suggest that the phase-separated PNIPAM thickness is 32 nm at 0.35 mW μm^{-2} and 50 nm for 0.53 mW μm^{-2}. A calculation based on numerical simulation suggests that a 100 nm Au NP core with a PNIPAM shell

Table 1. Experimental and Simulated Peak Shifts Dependent on Laser Peak Power Density[a]

laser peak power density/mW μm^{-2}	0.18	0.35	0.53
particle temperature (estimated)/K	302	308	315
shift (experimental)/nm	7 ± 6	34 ± 8	56 ± 9
shift (simulated)/nm	0	72	93

[a]The experimental peak shifts were determined from averages of 10 Au NPs. In simulations, a 100 nm diameter Au NP core with PNIPAM shell was assumed be supported on a glass substrate and surrounded by a water medium. The numerical estimates of the temperature were performed using COMSOL Multiphysics 5.1 (http://www.comsol.com).

(refractive index: 1.52[27]) thickness of 32 nm would give a 72 nm redshift in water. Likewise, a shell thickness of 50 nm would give a shift of 93 nm. Table 1 data show that the simulated peak shifts overestimated the experimental values because we assumed a dense PNIPAM shell such as that observed in the SEM images in Figure 2. In reality, the PNIPAM shell structure for the reversible phase separation can be sparsely distributed around a Au NP rather than densely packed.

For the experiments with glass substrates, we assume that PNIPAM aggregates form within the hot region surrounding the Au NP because the temperature is localized. As heat transfer only occurs near the particle, temperatures further outside the region are cooler than the LCST (Figure 1d). Hence, the PNIPAM molecules are dissolved and are freely mobile as random coil states. Therefore, the temperature-induced phase separation and confinement is the main reason for the LSPR shifts observed for the glass substrate. Previously, the Tsuboi group demonstrated with optical microscopy the plasmon-enhanced optical trapping of PNIPAM using a Au twin-nanopyramid structure.[28] They could trap a random coil form (hydrodynamic diameter, d_H = 11 nm) at a laser intensity of 10^3 W cm^{-2} (0.01 mW μm^{-2}) through plasmonic light enhancement, although a high laser intensity of $>10^7$ W cm^{-2} (1064 nm) would have been required for trapping in bulk D_2O solution. The Tsuboi group also observed trapping of a phase-separated globular aggregate with d_H = 100 nm at enhanced intensities $>3 \times 10^3$ W cm^{-2} where a temperature increase of 10 K was estimated. In our system, using a glass substrate, an optical trapping force may not be of prime importance for aggregation around a Au NP for the following reasons. The Au nanopyramid structure has an $|E|^2$ enhancement factor of 10^3−10^4, whereas a single 100 nm spherical Au NP has an enhancement factor of less than 20. Therefore, our laser intensities of 10^4 W cm^{-2} may not be feasible for optical trapping.

Recently, Orlishausen and Köhler observed the dynamic formation of PNIPAM aggregates that formed around laser-heated Au NPs.[29] The heating of a 250 nm diameter single Au NP in a 8−9 wt % PNIPAM solution with a focused illumination at a constant laser power of 51.9 mW (50−100 mW μm^{-2}) of wavelength 532 nm enabled the growth of the phase-separated aggregate from d < 10 μm at 0.3 s to $d \sim$ 100 μm at 500 s. After laser heating was stopped, the aggregates dissolved from the outside. Their aggregates are much larger than ours (10−100 μm vs ∼200 nm) for a laser peak power density 10−100 times higher than for the current study. In such circumstances, the melting and evaporation of Au NP, as well as vapor bubble formation around the heated NPs, are likely.[30] Hence, we infer that complicated high-temperature-induced

DOI: 10.1021/acs.jpcc.6b04265
J. Phys. Chem. C XXXX, XXX, XXX−XXX

processes may proceed in their system, and their observation is not compatible with ours.

We now focus our attention on the permanent encapsulation of Au NP by PNIPAM on a sapphire substrate. The observation recalls the recent study by Enders and co-workers who have demonstrated the encapsulation of Au NP by polyethylene glycol (PEG) or sodium dodecyl sulfate (SDS), forming a gold core−organic shell structure on laser illumination of Au NP.[31] However, an appreciably reduced laser intensity, approximately one-third, suffices for the permanent aggregation of PNIPAM on a Au NP compared with PEG or SDS, presumably because of the PNIPAM thermoresponse. For the mass transport mechanism in solution under thermal fields, three possible scenarios, thermophoresis, thermal convection, and Marangoni flow, can be postulated.

In thermophoresis, particles respond to the force of a temperature gradient by moving toward either colder or hotter regions.[32] The direction is determined by the thermal diffusion coefficient D_T, which when scaled by the common diffusion coefficient D yields the Soret coefficient $S_T = D_T/D$.[33] Given that their Soret coefficient is $S_T > 0$,[34,35] PNIPAM molecules are supposed to migrate from hot to cold regions. Previously, it was demonstrated that polymers with a positive Soret coefficient such as polystyrene in toluene can be repelled from the immediate vicinity of a Au NP when the particle dispersed in the polymer solution was heated to a stationary temperature by laser irradiation.[36] In our system with sapphire substrate, the calculated 2D radial temperature distribution around the Au NP is expected to be noncentrosymmetric (Figure 3a, right) because of a greater cooling effect of the substrate. Because of this, temperatures in the area below the particle appear to be appreciably higher than those above the particle, ($z = -100$ nm is the horizontal line below the particle, $z = 0$ nm the horizontal line above the particle, i.e., the water−substrate interface), as shown in Figure 3c. Nevertheless, the temperature gradients are directed (increase) radially from the outside medium toward the particle (Supporting Information S9), and PNIPAM molecules are expelled supposedly from the particle as stated in ref 36. Thus, for PNIPAM molecules to be attracted to Au NP, S_T should be negative. Sign changes as a function of temperature have been reported for PNIPAM in ethanol.[37] At this moment, whether thermophoresis is the only mechanism driving PNIPAM molecules to aggregate around the Au NP is hard to discern because D_T has not been determined at high temperatures of 340−360 K with extremely high temperature gradients of ∼1 K nm^{-1}, which are expected in the water/sapphire system. Note that thermophoresis may not occur for a glass substrate because of its centrosymmetric 2D temperature distribution (Figure 3a, left).

Next, the effect of convective flow is considered. Marangoni convection flow is a local mass flow created through nonuniform surface tension within a liquid and is proportional to the surface tension gradients.[38] Such gradients can be generated by a local change in variables such as composition and temperature. Because the surface tension of water decreases with temperature ($d\gamma/dT \simeq -0.144$ mN·m^{-1}·K^{-1}), the gradient in γ around the hot particle induces a thermal Marangoni flow, or thermocapillary flow. As shown in Figure 3a and 3c, temperature decreases along the interface between the particle and the medium, from below the particle and toward the substrate. Thus, Marangoni flow can be generated from the area below the particle toward the interface area of the particle and substrate (Figure 4). Besides the Marangoni flow, a

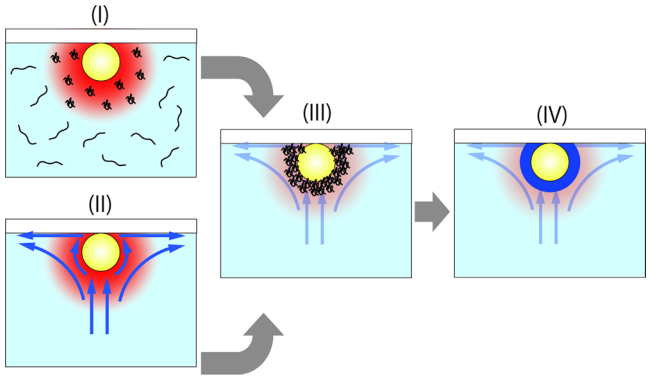

Figure 4. Schematic illustration of encapsulation. (I) Plasmonic-heating-induced phase transition of PNIPAM. (II) Generation of plasmonic-heating-induced Marangoni convective flow. (III) Deposition and aggregation of PNIPAM on a Au NP surface. (IV) Permanent phase separation of PNIPAM on a Au NP surface.

buoyancy-driven toroidal thermal convective flow can be induced by the temperature gradient between the upper interface near the particle and bulk water below the particle. This flow is relatively slow[31] but can continue to supply solute PNIPAM to the area near the particle, thus contributing to assist the Marangoni flow. Although quantitative treatment is so far not feasible, the synergetic effect of the two flows can promote the accumulation of PNIPAM around the top of the particle−substrate interface.

For the PNIPAM shell to form around a Au NP, the molecular flow must not only be adequate but also a certain attaching mechanism is required. A capillary phase separation of polymer solution has been shown to occur at the interface,[39,40] and in our case, the interface between the substrate and Au NP can act to promote this separation, aggregating the polymer. Under our experimental conditions, the particle temperatures are estimated to be from 340 and 360 K, well above the LCST, for power densities 3.5−5.3 mW μm^{-2}. With such high temperatures, the PNIPAM molecules around the NP can undergo not only phase separation but also vitrification resistant to remixing.[41] Such an assumption can be supported by the Raman spectroscopic measurement as shown in Supporting Information S10. The spectrum of the PNIPAM shell suggested that the heating-induced carbonization of the polymer was absent although isopropyl groups were partly eliminated. Accordingly, Both LCST- and capillary-assisted phase separation of PNIPAM must be responsible for the encapsulation around the Au NP on a sapphire substrate.

4. CONCLUSION

We demonstrated the optical sensing of temperature-induced phase separation of free PNIPAM molecules in solution exploiting a single Au NP immobilized on various substrates. We found the phase separation to be reversible or irreversible depending on the particle temperature and temperature shaping. With reversibility, single-particle LSPR has proven to be a powerful technique for *in situ* spectroscopic monitoring of the temperature-induced phase separation event. For PNIPAM, distinguishing spectroscopically the coiled and the globular states has been difficult in the past. For irreversible phase separation, encapsulation of a Au NP by various polymers can be useful in nanoarchitecture fabrication.

DOI: 10.1021/acs.jpcc.6b04265
J. Phys. Chem. C XXXX, XXX, XXX−XXX

■ ASSOCIATED CONTENT

Supporting Information

The Supporting Information is available free of charge on the ACS Publications website at DOI: 10.1021/acs.jpcc.6b04265.

Particle image with the corresponding histogram, experimental detail, AFM height profiles, additional scattering spectral changes, numerical simulation for a core−shell model supported on a substrate, SEM images for irradiation in PVP solution, 2D temperature-gradient distribution around a Au NP in water/sapphire, Raman spectra of PNIPAM shell (PDF)

■ AUTHOR INFORMATION

Corresponding Author

*Phone: 81-88-656-7389. Fax: 81-88-656-7598. E-mail: hashichem@tokushima-u.ac.jp.

Author Contributions

I.A. performed optical measurements. S.M. analyzed the data and performed the simulation. S.H. conceived and designed the experiment. S.H. wrote the manuscript with contributions from all authors. All authors have given approval to the final version of the manuscript.

Notes

The authors declare no competing financial interest.

■ ACKNOWLEDGMENTS

Financial support from JSPS KAKENHI (Grant No. 26286004) is gratefully acknowledged. We thank Satoshi Sugano for his technical support in SEM imaging. We thank Dr. Takayuki Uwada of Josai University for stimulating discussion.

■ REFERENCES

(1) Kreibig, U.; Vollmer, M. *Optical Properties of Metal Clusters*; Springer: Berlin, 1995.

(2) Link, S.; El-Sayed, M. A. Shape and Size Dependence of Radiative, Non-radiative and Photothermal Properties of Gold Nanocrystals. *Int. Rev. Phys. Chem.* **2000**, *19*, 409−453.

(3) Hartland, G. V. Optical Studies of Dynamics in Noble Metal Nanostructures. *Chem. Rev.* **2011**, *111*, 3858−3887.

(4) Hashimoto, S.; Werner, D.; Uwada, T. Studies on the Interaction of Pulsed Lasers with Plasmonic Gold Nanoparticles Toward Light Manipulation, Heat Management, and Nanofabrication. *J. Photochem. Photobiol., C* **2012**, *13*, 28−54.

(5) Baffou, G.; Quidant, R. Thermo-plasmonics: using Metallic Nanostructures as Nano-sources of Heat. *Laser Photonics Rev.* **2013**, *7*, 171−187.

(6) Qin, Z.; Bischof, J. C. Thermophysical and Biological Responses of Gold Nanoparticle Laser Heating. *Chem. Soc. Rev.* **2012**, *41*, 1191−1217.

(7) Dreaden, E. C.; Mackey, M. A.; Huang, X.; Kang, B.; El-Sayed, M. A. Beating Cancer in Multiple Ways Using Nanogold. *Chem. Soc. Rev.* **2011**, *40*, 3391−3404.

(8) Abadeer, N. S.; Murphy, C. J. Recent Progress in Cancer Thermal Therapy Using Gold Nanoparticles. *J. Phys. Chem. C* **2016**, *120*, 4691−4716.

(9) Kuhlicke, A.; Schietinger, S.; Matyssek, C.; Busch, K.; Benson, O. In Situ Observation of Plasmon Tuning in a Single Gold Nanoparticle During Controlled Melting. *Nano Lett.* **2013**, *13*, 2041−2046.

(10) Fava, D.; Winnik, M. A.; Kumacheva, E. Photothermally-triggered Self-assembly of Gold Nanorods. *Chem. Commun.* **2009**, 2571−2573.

(11) Urban, A. S.; Carretero-Palacios, S.; Lutich, A. A.; Lohmüller, T.; Feldmann, J.; Jäckel, F. Optical Trapping and Manipulation of Plasmonic Nanoparticles: Fundamentals, Applications, and Perspectives. *Nanoscale* **2014**, *6*, 4458−4474.

(12) Qiu, J.; Wei, W. D. Surface Plasmon-Mediated Photothermal Chemistry. *J. Phys. Chem. C* **2014**, *118*, 20735−20749.

(13) Fang, Z.; Zhen, Y. R.; Neumann, O.; Polman, A.; García de Abajo, F. J.; Nordlander, P.; Halas, N. J. Evolution of Light-Induced Vapor Generation at a Liquid-Immersed Metallic Nanoparticle. *Nano Lett.* **2013**, *13*, 1736−1742.

(14) Katayama, T.; Setoura, K.; Werner, D.; Miyasaka, H.; Hashimoto, S. Picosecond-to-Nanosecond Dynamics of Plasmonic Nanobubbles from Pump-Probe Spectral Measurements of Aqueous Colloidal Gold Nanoparticles. *Langmuir* **2014**, *30*, 9504−9513.

(15) Hashimoto, S.; Katayama, T.; Setoura, K.; Strasser, M.; Uwada, T.; Miyasaka, H. Laser-driven Phase Transitions in Aqueous Colloidal Gold Nanoparticles under High Pressure: Picosecond Pump−Probe Study. *Phys. Chem. Chem. Phys.* **2016**, *18*, 4994−5004.

(16) Schild, H. G. Poly(*N*-isopropylacrylamide): Experiment, Theory and Application. *Prog. Polym. Sci.* **1992**, *17*, 163−249.

(17) Wu, C.; Wang, X. Globule-to-Coil Transition of a Single Homopolymer Chain in Solution. *Phys. Rev. Lett.* **1998**, *80*, 4092−4094.

(18) Mock, J. J.; Barbic, M.; Smith, D. R.; Schultz, D. A.; Schultz, S. Shape Effects in Plasmon Resonance of Individual Colloidal Silver Nanoparticles. *J. Chem. Phys.* **2002**, *116*, 6755−6759.

(19) Underwood, S.; Mulvaney, P. Effect of the Solution Refractive Index on the Color of Gold Colloids. *Langmuir* **1994**, *10*, 3427−3430.

(20) Miller, M. M.; Lazarides, A. A. Sensitivity of Metal Nanoparticle Surface Plasmon Resonance to the Dielectric Environment. *J. Phys. Chem. B* **2005**, *109*, 21556−21565.

(21) Hofkens, Y.; Hotta, J.; Sasaki, K.; Masukhara, H.; Iwai, K. Molecular Assembling by the Radiation Pressure of a Focused Laser Beam: Poly(*N*-isopropylacrylamide) in Aqueous Solution. *Langmuir* **1997**, *13*, 414−419.

(22) Ishikawa, M.; Misawa, H.; Kitamura, N.; Fujisawa, R.; Masuhara, H. Infrared Laser-Induced Photo-Thermal Phase Transition of An Aqueous Poly(*N*-isopropylacrylamide) Solution in the Micrometer Dimension. *Bull. Chem. Soc. Jpn.* **1996**, *69*, 59−66.

(23) Tsuboi, Y.; Nishino, M.; Sasaki, T.; Kitamura, N. Poly(*N*-Isopropylacrylamide) Microparticles Produced by Radiation Pressure of a Focused Laser Beam: A Structural Analysis by Confocal Raman Microspectroscopy Combined with a Laser-Trapping Technique. *J. Phys. Chem. B* **2005**, *109*, 7033−7039.

(24) Honda, M.; Saito, Y.; Smith, N. I.; Fujita, K.; Kawata, S. Nanoscale Heating of Laser Irradiated Single Gold Nanoparticles in Liquid. *Opt. Express* **2011**, *19*, 12375−12383.

(25) Kusolkamabot, K.; Sae-ung, P.; Niamnont, N.; Wongravee, K.; Sukwattanasinitt, M.; Hoven, V. P. Poly(*N*-isopropylacrylamide)-Stabilized Gold Nanoparticles in Combination with Tricationic Branched Phenylene-Ethynylene Fluorophore for Protein Identification. *Langmuir* **2013**, *29*, 12317−12327.

(26) Setoura, K.; Okada, Y.; Werner, D.; Hashimoto, S. Observation of Nanoscale Cooling Effects by Substrates and the Surrounding Media for Single Gold Nanoparticles Under CW-Laser Illumination. *ACS Nano* **2013**, *7*, 7874−7885.

(27) Reufer, M.; Díaz-Leyva, P.; Lynch, I.; Scheffold, F. Temperature Sensitive Poly(N-Isopropyl-Acrylamide) Microgel Particles: A Light Scattering Study. *Eur. Phys. J. E: Soft Matter Biol. Phys.* **2009**, *28*, 165−171.

(28) Toshimitsu, M.; Matsumura, Y.; Shoji, T.; Kitamura, N.; Takase, M.; Murakoshi, K.; Yamauchi, H.; Ito, S.; Miyasaka, H.; Nobuhiro, A.; et al. Metallic-Nanostructure-Enhanced Optical Trapping of Flexible Polymer Chains in Aqueous Solution As Revealed by Confocal Fluorescence Microspectroscopy. *J. Phys. Chem. C* **2012**, *116*, 14610−14618.

(29) Orlishausen, M.; Köhler, W. Forced Phase Separation by Laser-Heated Gold Nanoparticles in Thermoresponsive Aqueous PNIPAM Polymer Solutions. *J. Phys. Chem. B* **2015**, *119*, 8217−8222.

DOI: 10.1021/acs.jpcc.6b04265
J. Phys. Chem. C XXXX, XXX, XXX−XXX

(30) Nishimura, Y.; Nishida, K.; Yamamoto, Y.; Ito, S.; Tokonami, S.; Iida, T. Control of Submillimeter Phase Transition by Collective Photothermal Effect. *J. Phys. Chem. C* **2014**, *118*, 18799−18804.
(31) Enders, M.; Mukai, S.; Uwada, T.; Hashimoto, S. Plasmonic Nanofabrication Through Optical Heating. *J. Phys. Chem. C* **2016**, *120*, 6723−6732.
(32) Duhr, S.; Braun, D. Why Molecules Move along a Temperature Gradient. *Proc. Natl. Acad. Sci. U. S. A.* **2006**, *103*, 19678−19682.
(33) Würger, A. Thermal Non-equilibrium Transport in Colloids. *Rep. Prog. Phys.* **2010**, *73*, 126601.
(34) Kita, R.; Wiegand, S. Soret Coefficient of Poly(*N*-isopropylacrylamide)/Water in the Vicinity of Coil-Globule Transition Temperature. *Macromolecules* **2005**, *38*, 4554−4556.
(35) Wongsuwarn, S.; Vigolo, D.; Cerbino, R.; Howe, A. M.; Vailati, A.; Piazza, R.; Cicuta, P. Giant Thermophoresis of Poly(*N*-isopropylacrylamide) Microgel Particles. *Soft Matter* **2012**, *8*, 5857−5863.
(36) Schwaiger, F.; Zimmermann, W.; Köhler, W. Transient Cage Formation Around Hot Gold Colloids Dispersed in Polymer Solutions. *J. Chem. Phys.* **2011**, *135*, 224905.
(37) Kita, R.; Kircher, G.; Wiegand, S. Thermally Induced Sign Change of Soret Coefficient for Dilute and Semidilute Solutions of Poly(*N*-isopropylacrylamide) in Ethanol. *J. Chem. Phys.* **2004**, *121*, 9140−9146.
(38) Gugliotti, M.; Baptista, M. S.; Politi, M. J. Laser-Induced Marangoni Convection in the Presence of Surfactant Monolayers. *Langmuir* **2002**, *18*, 9792−9798.
(39) Wennerström, H.; Thuresson, K.; Linse, P.; Freyssingeas, E. Long Range Attractive Surface Forces Due to Capillary-Induced Polymer Incompatibility. *Langmuir* **1998**, *14*, 5664−5666.
(40) Olsson, M.; Linse, P.; Piculell, L. Capillary-Induced Phase Separation in Binary and Quasi-Binary Polymer Solutions. A Mean-Field Lattice Study. *Langmuir* **2004**, *20*, 1611−1619.
(41) Van Durme, K.; Van Assche, G.; Van Mele, B. Kinetics of Demixing and Remixing in Poly(*N*-isopropylacrylamide)/Water Studied by Modulated Temperature DSC. *Macromolecules* **2004**, *37*, 9596−9605.

DOI: 10.1021/acs.jpcc.6b04265
J. Phys. Chem. C XXXX, XXX, XXX−XXX